Cold Regions Science and Technology 146 (2018) 43–52

Contents lists available at ScienceDirect

Cold Regions Science and Technology

journal homepage: www.elsevier.com/locate/coldregions

Reduction of snow albedo from vehicle emissions at Portillo, Chile

Francisco Cereceda-Balic[a], Víctor Vidal[a], Hans Moosmüller[b], Magín Lapuerta[c,*]

[a] Center for Environmental Technologies (CETAM), Universidad Técnica Federico Santa María, Av. España 1680, Valparaíso, Chile
[b] Desert Research Institute, Nevada System of Higher Education, Reno, NV 89512, USA
[c] E.T.S. Ingenieros Industriales, Universidad de Castilla-La Mancha, Avda. Camilo José Cela s/n, 13071 Ciudad Real, Spain

ABSTRACT

Only scarce literature exists on the effect of direct deposition of vehicle particulate matter emissions onto snow surfaces with well-quantified sources and atmospheric conditions. Local emissions from vehicles in the surroundings of ski resorts not only reduce the whiteness of the snowy landscape affecting the attractiveness to visitors, but also modify the onset of snowmelt and thus the environmental equilibrium of the local area and of the surrounding region. The changes in albedo observed at Portillo, in the Chilean Andes, were an increase of around 0.17 units after a heavy snowfall (20 cm accumulation), an increase of around 0.07 after a prolonged lighter snowfall (10 cm accumulation), and a mean decrease of around 0.08 units per day with heavy traffic (around 2000 vehicles per day). Other parameters such as wind velocity and direction did not greatly affect the snow albedo during this study because the wind direction was fairly constant due to the terrain restriction. It is difficult to estimate how much the snow metamorphism and melting contributed to the observed decrease. The albedo changes observed are helpful to confirm the close cause-effect relationship between these parameters and the snow albedo, and to foresee that traffic restriction may allow for more stable snowpack conditions. The case study presented here can be extrapolated to other vehicle-contaminated snow areas, thus examining their contribution to snow radiative forcing and climate change at multiple scale.

1. Introduction

Snow albedo is of great importance for snow energy balance, metamorphism, and timing of snowmelt. All of these effects are of the essence for downstream reservoir operation, irrigation, and flood control, and for the operation of ski areas (Painter et al., 2010). In the visible and the sub - 1 μm spectral region, snow albedo is largely controlled by light absorbing impurities; above 1 μm wavelength by snow grain size (Gardner & Sharp, 2010). Black carbon aerosols have the strongest light absorption per mass and are therefore of prime interest because of their great ability in reducing snow albedo (Moosmüller et al., 2009).

Numerous studies have been published about the reduction of snow albedo by ambient black carbon aerosol deposition, especially in the Himalayas (Jacobi et al., 2015; Ginot et al., 2015; Ming et al., 2008, 2009), but also in other areas such as Sierra Nevada (USA) (Lee & Liou, 2012; Sterle et al., 2013), Hokkaido island (Aoki et al., 2011), Alpes (Dumont et al., 2017), etc. However, in studies made in remote areas, black carbon concentrations are generally too low to quantify their influence on snow albedo. In addition, some studies have examined the effect of well-controlled soot deposition on artificial snowpacks (Brandt et al., 2011; Hadley & Kirchstetter, 2012), but these studies were made far from real-world conditions, may not include realistic sources, deposition mechanisms, or realistic snow characteristics.

Also experimental and modeling studies have been published showing the effect of many different parameters on the snow albedo (Gardner & Sharp, 2010; Aoki et al., 2003; Qu & Hall, 2007, 2014). These studies can be classified into: a) studies examining the direct effect of snow physical properties, including the effects of snow grain size or shape (Gardner & Sharp, 2010; Aoki et al., 2011; Hadley & Kirchstetter, 2012; Aoki et al., 2003; Painter et al., 2012; Nolin & Dozier, 2000) or specific surface area of the snow crystals (Dumont et al., 2017; Domine et al., 2006), presence of liquid water (Dumont et al., 2017), snow aging (elapsed time after snowfalls) (Lee & Liou, 2012; Aoki et al., 2003), and snowpack depth (Sterle et al., 2013; Aoki et al., 2003); b) studies examining the indirect effect of snow physical properties derived from solar heating profile (Aoki et al., 2011), ambient temperature (Aoki et al., 2011, 2003) or snow surface temperature (Lee & Liou, 2012; Aoki et al., 2003; Qu & Hall, 2007); c) studies about the effect of the spectral or angular characteristics of the illumination, such as solar zenith angle (Painter et al., 2010; Gardner & Sharp, 2010; Wang & Zender, 2010), terrain slope (Dumont et al.,

* Corresponding author.
E-mail address: magin.lapuerta@uclm.es (M. Lapuerta).

https://doi.org/10.1016/j.coldregions.2017.11.008
Received 8 May 2017; Received in revised form 14 November 2017; Accepted 18 November 2017
Available online 21 November 2017
0165-232X/

2017), water vapour concentration (Manninen et al., 2012) or cloud thickness (Gardner & Sharp, 2010), ozone concentration in the atmosphere (Manninen et al., 2012), aerosol optical depth (Aoki et al., 2011), and black-carbon concentration in the atmosphere (Jacobi et al., 2015; Ginot et al., 2015); and finally, d) studies about effect of the presence of impurities in the snow, such as mineral dust concentration (Painter et al., 2010; Jacobi et al., 2015; Ginot et al., 2015; Aoki et al., 2011), or soot concentration in the snow (Jacobi et al., 2015; Ginot et al., 2015; Ming et al., 2008, 2009; Sterle et al., 2013; Brandt et al., 2011; Hadley & Kirchstetter, 2012). In most of the latter studies, the source of soot was unknown or it was produced synthetically.

However, we are not aware of any studies of the effect of direct particulate matter deposition from vehicle traffic onto snow surfaces with well-characterized emitting sources and atmospheric conditions. Particulate matter mass in vehicle emissions is dominated by black carbon (or elemental carbon, or soot) and organic carbon (Allen et al., 2001), with the former dominating particulate matter light absorption and consequently snow albedo reduction and snow surface warming after deposition (Flanner et al., 2009).

Here, we selected an area where snow contamination is dominated by emissions from vehicles passing close to the measurement point and we analysed the relation between contamination source, atmospheric conditions, and reduction of the snow albedo over a one-week period. In this situation, nearby, real-world, anthropogenic emissions are expected to induce measurable variations of snow albedo, thereby helping to bridge between artificial deposition studies and studies in remote areas.

The area selected was near Portillo, a Chilean ski resort located very close to the Paso Los Libertadores at more than 2800 m altitude, where the border between Chile and Argentina is located. The road accessing Portillo and connecting Chile and Argentina across the border pass has a very high traffic density, with a large number of passenger cars and trucks travelling in both directions. However, during heavy snowfalls in winter, the access for vehicles is often restricted. In this area road traffic is the main source of contamination and relative contributions of other sources are negligible. The concentrated contamination from vehicle emissions in this area not only reduces the whiteness of the snowy landscape, thereby affecting the attractiveness of the Portillo resort to skiers and visitors, but also modifies the onset of snowmelt thus disturbing the environmental equilibrium of the local area and region. In addition to this, the case study presented here can also be extended to other vehicle-contaminated snowy areas, thereby helping to quantify their contribution to radiative forcing (Sterle et al., 2013; Hall, 2004; Hall & Qu, 2006) and to the hydrological cycle (Qian et al., 2014) on different scales.

2. Experimental equipment and methods

2.1. Determination of snow albedo, and sky and snow skin temperature

A portable radiometer Kipp & Zonen CNR4, equipped with a data logger Logbox SD, was used for the measurements. This radiometer includes a pyranometer (with sensitivity from 10 to 20 μV/W/m^2 and maximum uncertainty of 5% at 95% confidence level), covering the solar spectral range from 300 to 2800 nm, and a pyrgeometer (with sensitivity from 5 to 15 μV/W/m^2, and maximum uncertainty of 10% at 95% confidence level), covering the thermal infrared spectral range from 4500 to 42000 nm. Both include sensors for down-welling and up-welling radiation, which were located 1.85 m above the ground and around 1.2 m above the horizontal snow surface (the thickness of the snowpack varied between 55 and 80 cm during the measurement period). The down-welling pyranometer measured the incident solar irradiance and the up-welling one measured the irradiance reflected by the snow surface. The broadband albedo was determined as the ratio between the reflected and incident irradiance. The same procedure was used to determine the albedo of the ground below the snowpack from measurements made after all the snow was melted at the beginning of southern spring.

Snow surface temperature was deduced from the longwave measurements from the pyrgeometer using the Stefan-Boltzmann law. The incident down-welling irradiance W_{down} was used to estimate the apparent sky temperature (which is in fact a brightness temperature), and the up-welling irradiance W_{up} was used to estimate the apparent snow skin temperature, considering both sky and snow as black bodies. For a more precise estimate of the snow temperature, Kirchhof's law was used to take the thermal infrared emissivity ε and reflectivity $(1 - \varepsilon)$ of the snow into account, yielding the apparent snow temperature as (Aoki et al., 2003):

$$T'_{sky} = \left(\frac{W_{down}}{\sigma}\right)^{1/4};$$
$$T_{snow} = \left(\frac{W_{up} - W_{down}(1-\varepsilon)}{\varepsilon\sigma}\right)^{1/4} \quad (1)$$

where σ is the Stefan Boltzmann constant and we are assuming a snow emissivity of 0.97, as proposed by Kondo and Yamazawa (Kondo & Yamazawa, 1986).

2.2. Weather conditions

Temperature and relative humidity were measured with a temperature/humidity Onset S-THB-M002 sensor (accuracy ± 0.21 °C and ± 2.5%, respectively) and barometric pressure was measured with Onset S-BPB-CM50 sensor (accuracy ± 3 mbar). Absolute humidity was calculated from relative humidity, ambient temperature, and pressure. Wind direction and speed were measured with Onset S-WDA-M003 and S-WSB-M003 sensors (accuracies ± 5°. and ± 1.1 m/s), respectively. All sensors were located on the roof of the Nunatak scientific platform, a portable laboratory-refuge (2.3 m high) belonging to CETAM (Universidad Técnica Federico Santa María) and designed for research campaigns under extreme conditions, with autonomous electric supply from photovoltaic panels.

Data were recorded every minute with a HOBO U30 weather monitoring station during the week of 21st July to 28th July 2016. This week was selected because snowfall was predicted during the week. Daily information about snowfall was obtained from the Ski Portillo historical report (http://www.onthesnow.com/chile/ski-portillo/historical-snowfall.html).

2.3. Location, traffic information, and fuels

The exact measurement location was: latitude: − 32° 50 min 43 s, longitude: 70° 07 min 47 s, and altitude: 2813 m. Both the radiometer and the scientific platform were installed in an area occupied by the Escuela de Alta Montaña of the Chilean Army, in a sector that was kept free of pedestrians and vehicle traffic. The road rises up from Los Andes city to around this point, as shown in Fig. 1, and continues rising up to Paso Los Libertadores, the location of the Chilean-Argentinian border (right at the East side of the image).

The traffic information for the days of the measurement campaign was provided by the Chilean National Service of Customs. The information consists of the daily numbers of passenger cars, buses, and trucks travelling in both directions.

Argentinian diesel and gasoline fuels for transport are categorized as Grade 2 or Grade 3, with most of the trucks and buses using diesel fuel Grade 2 and most of the passenger cars using gasoline Grade 2. The Argentinian quality standard establishes different sulfur content limits for diesel fuel Grade 2 depending on the population density of the area. The Cuyo region of Argentina, which connects to Chile through Portillo, is a low-density region. From June 2016 (Resolution 5/2016, which modifies previous resolution 1283/2006 (www.infoleg.ar)), the sulfur content is limited to 1500 ppm for diesel Grade 2 and 150 ppm for gasoline Grade 2. Chilean specifications for diesel and gasoline fuel

Fig. 1. Layout of the road surrounding the measurement point (marked with a red arrow). (For interpretation of the references to colour in this figure legend, the reader is referred to the web version of this article.)

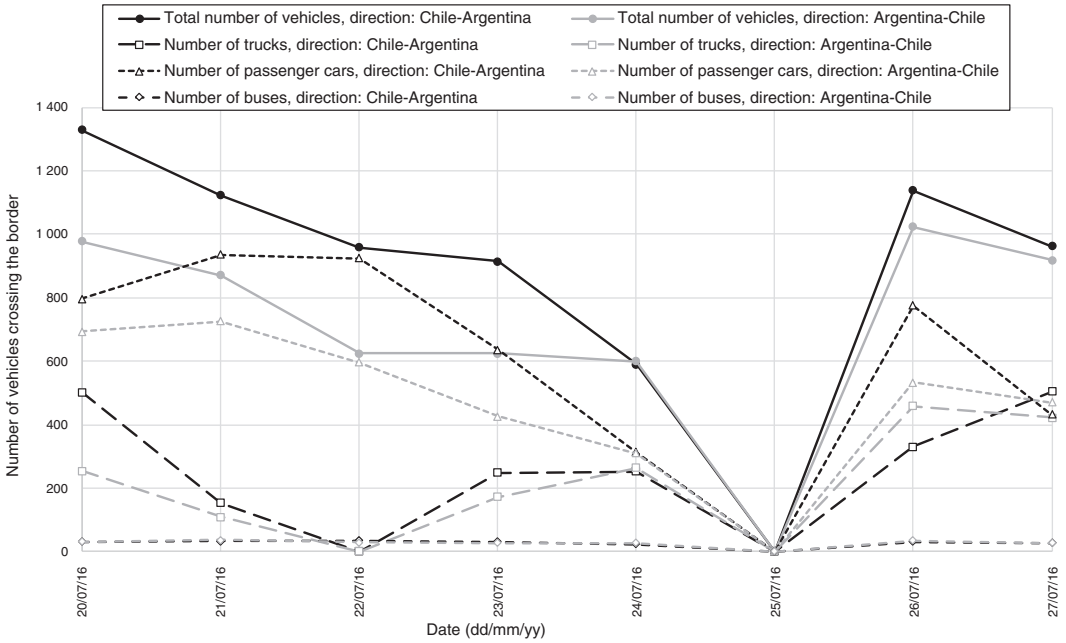

Fig. 2. Traffic intensity in both directions, disaggregated by type of vehicles, during the measurement week.

(D.S. No 60 from 2012) are more stringent than Argentinian ones, with 15 ppm sulfur for gasolines and diesel Grade B-1 fuel in the metropolitan Santiago region (around Santiago city) and 50 ppm sulfur for diesel Grade B-1 fuel in the rest of the country (www.leychile.cl). Although Portillo belongs to the Valparaíso region, it is close to the metropolitan Santiago region, and it is expected that many trucks and buses use ultra-low (15 ppm) sulfur diesel fuels. With regard to other fuel properties contributing to particulate matter emissions, such as distillation curve, aromatic content, density, or cetane number, the quality of Chilean diesel fuels is also better. On the contrary, oxygenated biofuels (contributing to the reduction of particulate matter emissions) are more common in Argentina than in Chile. In general, it can be assumed that vehicles travelling up from Chile up towards the border used cleaner fuels than those travelling from Argentina downwards, but the former ones were running in much more particle-emitting conditions (higher engine loads) than the latter ones.

2.4. Numerical albedo simulations

The NOAA (National Oceanic and Atmospheric Administration) solar position calculator, from the U.S. Earth System Research Lab (http://www.esrl.noaa.gov/gmd/grad/solcalc/azel.html), was used to

determine the solar elevation and zenith angles at the measurement point during the measurement campaign. These angles were used as input into the SNICAR (Snow, Ice and Aerosol Radiation) code (http://snow.engin.umich.edu/snicarcode/), from the University of Michigan, which was used to calculate the expected variation of snow albedo during the daytime for clear sky, and typical conditions of the snowpack.

3. Results and discussion

3.1. Weather and traffic intensity

The information published by Ski Portillo historical report (http://www.onthesnow.com/chile/ski-portillo/historical-snowfall.html) during the measurement week was 20 cm snow accumulation for the first snowfall (23 July) and 10 cm snow accumulation for the second one (attributed entirely to 25 July). The traffic intensity during this week is shown in Fig. 2. As observed, passenger cars were most common in both directions, followed by trucks, with the number of buses being minor. Traffic was restricted to trucks during 22 July due to snow forecast. An intense snowfall finally occurred during the following night (from 2 am to 9 am of 23 July). Two days later (25 July) traffic was restricted for all kinds of vehicles. Here, the snowfall started quite intensely the day before (24 July) at 2 pm and became lighter after a few hours, but continued until ~11 pm of 25 July. No other traffic restrictions were in place during the remainder of the week. During the week studied, traffic from Argentina downward towards Chile was always ~20% lower than traffic in the opposite uphill direction (806 vehicles per day compared to 1002 vehicles per day without traffic restrictions, on average). The overall weather conditions and the snowfalls and traffic details are summarized in Table 1.

3.2. Ambient, sky and snow skin temperatures, and humidity

Ambient temperatures were increasing during the morning (Fig. 3), reaching peaks sometime after noon (between 12:20 and 13:50 h, local standard time) with variable values (between 5 °C and 17 °C, except for day 25 July when the peak temperature was −2 °C), and then decreasing with minima of 0 °C (except 25 July, when temperatures dropped to −10 °C). From down- and up-welling irradiances, the apparent temperatures of sky and snow skin were obtained. As observed, the effect of the non-absorbed incident radiation and the non-unity emissivity are minor and just lead to a slight increase with respect to the apparent snow temperature. Only results from two days are shown as examples of sunny (21 July until 13.30) and cloudy times (21 July from 13.30 and 22 July).

Fig. 3 shows that snow temperature peaks are delayed with respect to those of ambient temperature as a consequence of the thermal inertia of the snow. Increases in the snow skin temperature during the afternoon are limited by snow melting, which keeps temperature at a maximum of 0 °C, with much lower oscillations than during the other parts of the day. With regard to the apparent sky temperature, it tends to follow the snow temperature in general, but it is clearly increased by snow melting, probably because the associated increase in water vapour concentration tends to heat the ambient layer above the measuring location.

An example of relative and absolute humidity is shown in Fig. 4 for the same two days. During sunlight hours, ambient temperature varies similarly to absolute humidity but oppositely to relative humidity, whereas during dark hours, trends are less clear. Also, the presence of clouds contributes to increase of both relative and absolute humidities, albeit with a much larger effect on the relative humidity than on the absolute one. Snow melting may also have some effect on increasing humidity. Finally, during snowfall, relative humidity remained above 90% (reaching 97%) regardless of ambient temperature. The relation between relative humidity and ambient temperature can better be

Table 1
Summary of traffic and weather conditions along the measurement week.

Day of July 2016	21	22	23	24	25	26	27
Traffic	Intense (trucks and cars)	Medium (restricted to trucks, Intense for cars)	Intense (trucks and cars)	Medium (intense for trucks and light for cars)	Restricted	Intense (trucks and cars)	Intense (trucks and cars)
Snowfall	No	No	Very intense during morning (20 cm accumulation)	Intense during afternoon	Light during all day (10 cm accumulation)	None	None
Weather	Sunny	Clouds in the afternoon	Snowy (morning), and cloudy (afternoon)	Cloudy (morning) and snowy (afternoon)	Snowy, cloudy and cold	Very sunny and very cold	Cloudy (morning) and sunny (afternoon)

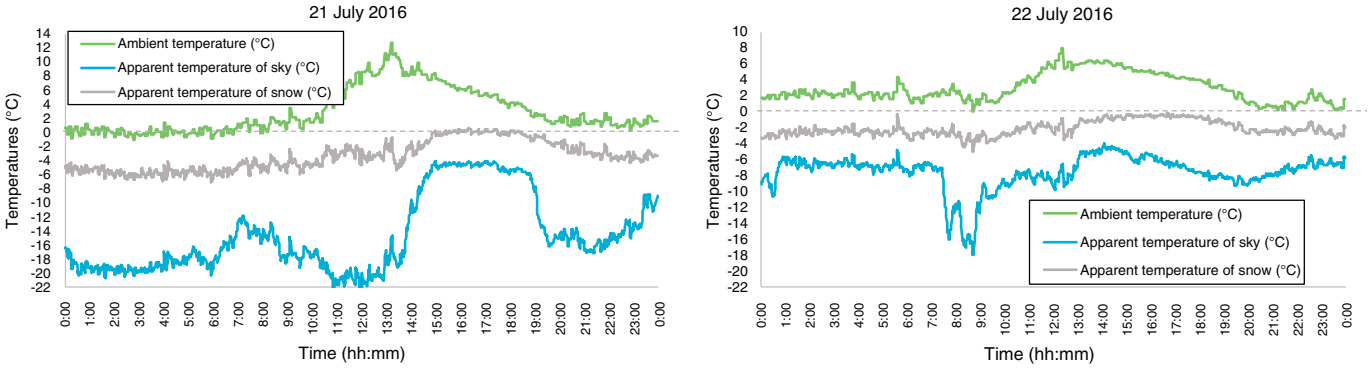

Fig. 3. Ambient temperature measured and skin snow and sky temperatures derived from down- and up-welling infrared radiance for 21 and 22 July 2016.

observed in Fig. 5, which displays data for the whole week. As observed in the figure, the evening-night-morning after the second snowfall (between 25th and 26th July) was exceptionally cold, and the next day was the sunniest day.

3.3. Wind speed and direction

Wind was mainly channelled from the North-East towards the South-West or vice versa (around 30° or 210°), as a consequence of the terrain, which leaves an open corridor in this direction. From 5-minute time-resolved wind direction and speed data, a wind rose was constructed, as presented in Fig. 6, left. It includes the statistics (length of the sectors) for the wind direction from which the wind blows and the wind speed (colour code) for the whole week. It can be observed that wind speeds higher that 3.6 m/s were exceptional especially when blowing from the North-East, and remained always below 6 m/s. Such low wind speeds prevented any snowdrift during the study. Daily-averaged values are shown in Fig. 6, right, where again the coloured dots indicate the direction from which the wind blows. For all days of the week, the preferential wind direction was on average approximately parallel to the traffic direction on the section of the road nearest to the measuring point (see Fig. 1), meaning that particle emissions from vehicles are not preferentially blown towards the measuring point.

3.4. Incident and reflected solar radiation and snow albedo

The incident and reflected solar irradiance [300–2800 nm] measured during the seven campaign days is shown in Fig. 7. Sudden changes observed on sunny days correspond to the exact times when the measurement site switches between being shadowed by the mountains and being illuminated by direct sunlight. The derived daytime snow broadband albedo is shown in Fig. 8. From both figures, it can be observed that the reflected irradiance is smaller than the incident one (albedo values below one) during daytime, except during snowfall. Intense snowfall led to measured snow albedos higher than unity even during daytime. A likely explanation is the snow accumulation on the up-looking sensor measuring down-welling (i.e. incident) radiation but not on the down-looking sensor measuring up-welling (i.e. reflected) radiation. This explanation is in agreement with the observation that light snowfalls did not lead to albedo values higher than

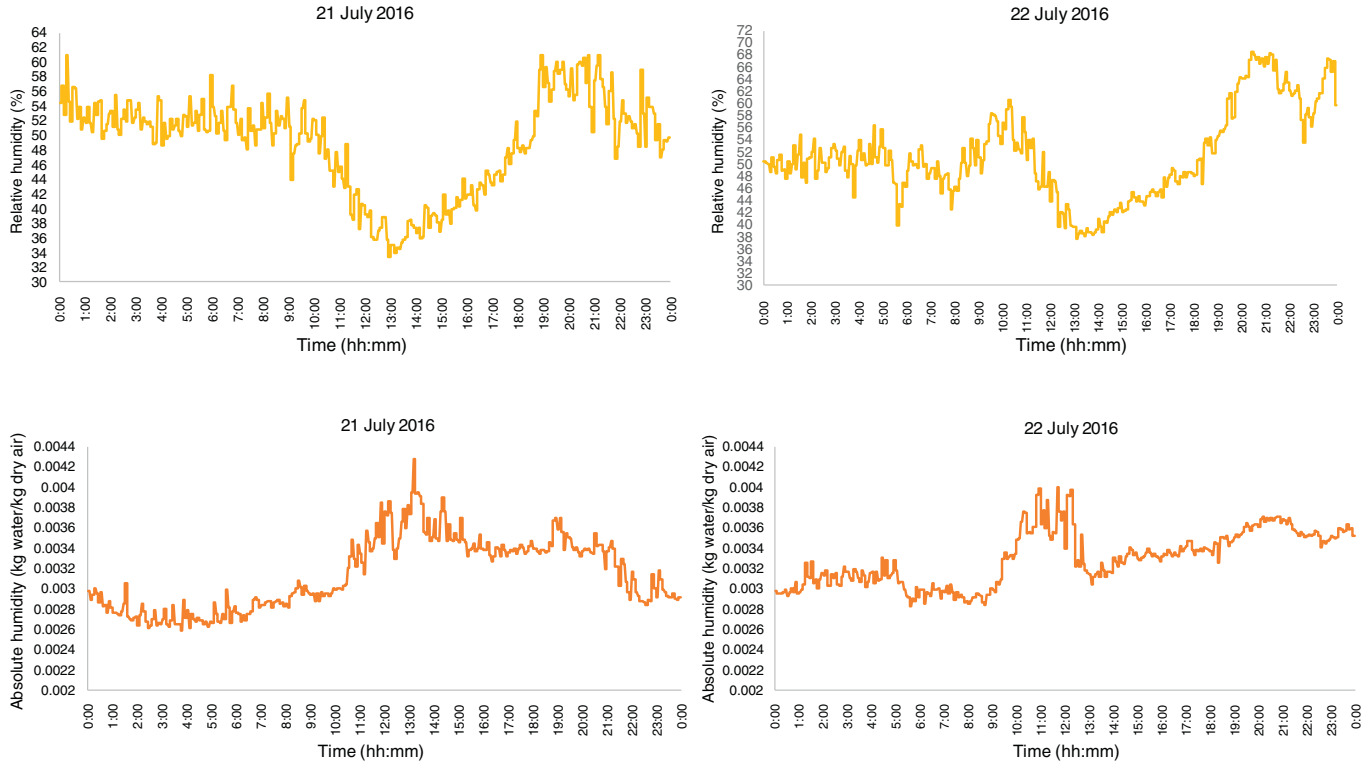

Fig. 4. Relative and absolute humidities for 21 and 22 July 2016.

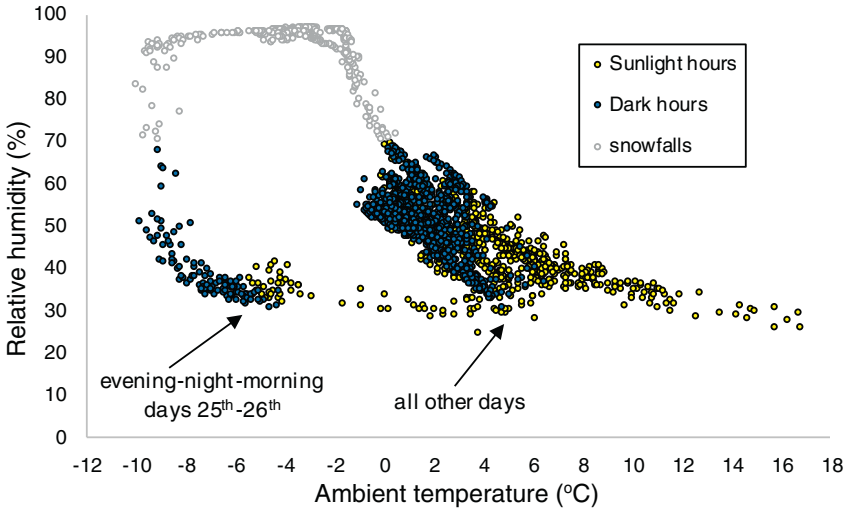

Fig. 5. Relation between relative humidity and ambient temperature for the whole week.

unity, probably because they caused no or only minor snow accumulation on the up-looking sensor.

As shown in Fig. 8, the broadband albedo decreased from values higher than unity during the night, at which there is very little incident and reflected solar radiation, and therefore, the ratio between the two (the albedo) is largely determined by minor zero offsets in the measurements of incident and reflected solar radiation. It must be noted that the accuracy of radiometers is low for low solar elevations (Picard et al., 2016). From dawn onwards, the albedo, first rapidly, then more slowly, decreased until a plateau was reached for the mid-day hours. During the early afternoon, the albedo increased slowly with time, followed by a sudden increase just before sunset. Similar patterns were observed during clear and cloudy conditions. On days with no snowfalls and with heavy traffic, especially with large number of trucks travelling uphill, such as 21, 26 and 27 July, the snow albedo decreased during the day with respect to the expected diurnal pattern (see below) as a consequence of soot deposition. However, this decrease was neither uniform nor smooth, as a consequence of the variability of traffic intensity, wind speed and direction, deposition mechanism, etc., during the day.

3.5. Albedo of the underlying surface

After snowfalls occurred on 23 and 24–25 July, only a minor snowfall occurred on 2 August with 5 cm snow accumulation. After this event, sunny days dominated the weather and the snowpack was progressively melting until completely disappearing by the end of the southern winter. Five days at the beginning of the southern spring (from 22 to 26 September) were selected to determine the albedo of the ground, which was assumed to be that of the underlying surface for the days of the snow albedo campaign. Results are shown in Fig. 9 for daytime. In this case, the albedo decreased from values higher than unity after dawn to rather constant values between 0.1 and 0.2, and then it increased again after sunset. This pattern was much more repetitive than that observed for the snow. The average albedo calculated from 9:00 to 17:30 for these five days was 0.146 with a standard deviation of 0.003. This value was used for the albedo calculation as explained below.

3.6. Confirmation of daily trend for snow albedo

To investigate the diurnal patterns of the measured snow albedo, the elevation and zenith angles were determined at the measurement point for 22 July as an example. They are shown in Fig. 10 with dashed lines. These angles, together with the information about the snowpack thickness in the radiometer location (70 cm on average), the albedo of the underlying surface measured two months later (0.146, see previous section), the snowpack density (measured from a test pit dug on 28 July, resulting in 279 kg/m^3 in the upper layer), the grain size (estimated as 500 µm from snow photographs), and the uncoated black carbon concentration (assumed as 200 ppb for this calculation), were used as input into the SNICAR model (http://snow.engin.umich.edu/snicarcode/) to simulate the snow albedo. Modelled and experimental results for 22 July are also shown in Fig. 10 with solid lines (blue and

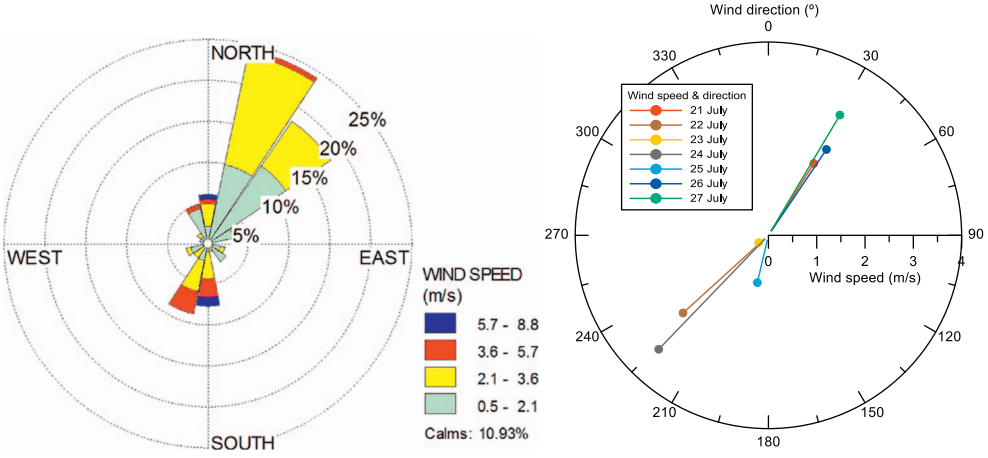

Fig. 6. Wind rose for speed and direction throughout the whole week (left) and daily-average wind speed and direction values (right).

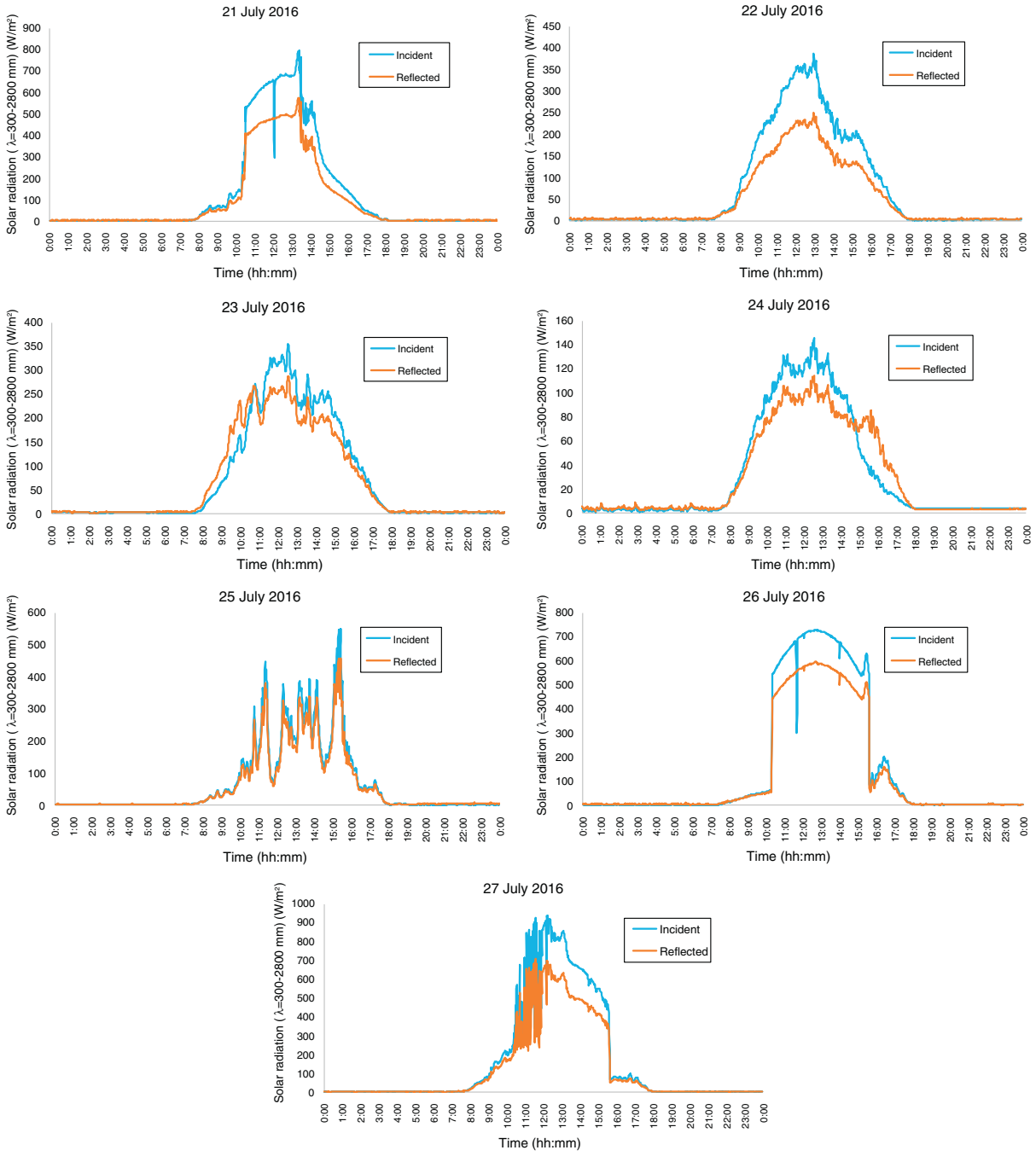

Fig. 7. Incident and reflected daily solar irradiance measured during 21 to 27 July 2016.

brown respectively). Modelled and measured results are in good agreement between 10:00 and 17:30, and both are in qualitative agreement with trends predicted by theoretical equations (Giddings & LaChapelle, 1961). It was checked from the records that differences in this period correspond to cloudy hours. For example, the highest difference (0.03 units) occurred at 14:30 h, which corresponds with the highest drop in incident radiation. This can be explained because clouds preferentially absorb near-infrared wavelengths, shifting the spectral distribution of incident radiation towards shorter wavelengths (where the snow albedo is higher), thereby increasing the snow broadband albedo. Such increase with increasing cloud cover was confirmed with the parametrization model proposed by Gardner and Sharp (Gardner & Sharp, 2010). However, at early and late hours, measured values are much larger than modelled ones, which could be explained by the complex topography of the surrounding terrain, by inaccuracies in the horizontality of the sensors or of the snow surface, and by errors in both or either measurements or modeling for large zenith angles. In any case, this general good agreement confirms the reliability of the observed trends.

3.7. Albedo history and interpretation

Finally, the broadband albedo history along the measurement week is shown in Fig. 11, including icons for the main factors affecting the snow albedo. For averaging the daily snow albedo, only the time period from 11.30 to 14.00 was used, because it was the only period not affected by any heavy snowfall on any day (see Figs. 7 and 8). In addition, the average albedo along this time period represents the middle-day

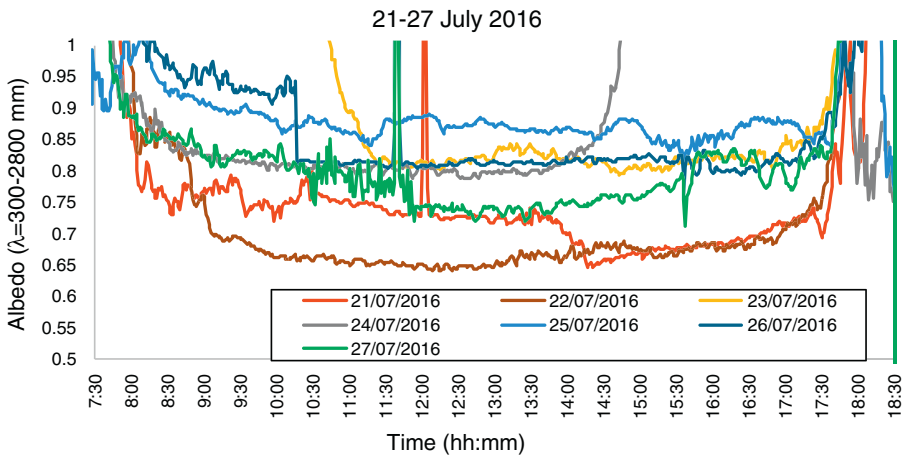

Fig. 8. Broadband daytime snow albedo for the week-long campaign.

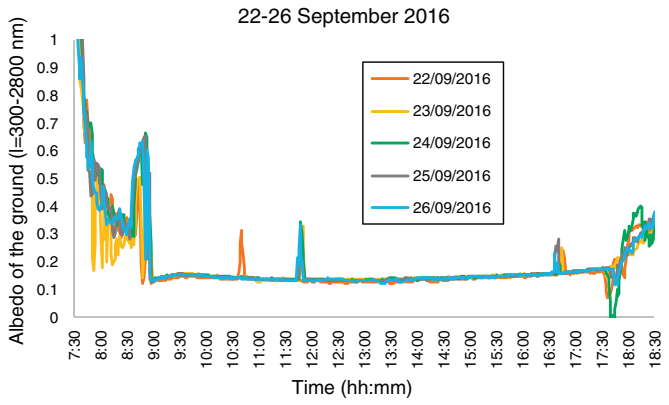

Fig. 9. Broadband daytime ground albedo for five days after snow-melt.

plateau with excellent agreement between model and measurements. As observed, increases in broadband albedo occurred on days after snowfalls and decreases correspond to periods free of snowfall and with exposure to traffic. More details of the increases and decreases in the average albedo are:

- On 23 July, an albedo increase of 0.17 units was measured with respect to the previous day, as a consequence of the heavy snowfall that occurred during the morning of that day (20 cm of snow accumulation). On 25 July, another albedo increase of 0.07 units was measured as a consequence of the lighter but longer snowfall event that occurred the previous afternoon and on the same day (10 cm of snow accumulation).
- On the contrary, on 22 July, an albedo decrease of 0.08 units was measured with respect to the previous day as a consequence of intense traffic of around 2000 vehicles/day and of snow melting in the afternoon. On 24 July, the albedo was only reduced by 0.02 units with respect to the previous day because only half of 23 and 24 July was free of snowfall, and because the traffic was not heavy. On 26 July, the reduction was 0.04 units with respect to the previous day, because traffic was fully restricted the previous day and thus only contributed to albedo reductions during the first part of 26 July. On 27 July, the reduction was 0.08 units because there was intense traffic exposure during the whole day, as well as snow melting in the afternoon. However, it is likely that the snow melting and the consequent change in grain size due to snow metamorphism also contributed to this decrease, as demonstrated and quantified by Flanner and Zender (Flanner & Zender, 2006).

No average rates of increase or decrease have been proposed because none of these effects is expected to be linear. In fact, the masking effectivity of clean snow (with higher specific surface area and lower grain size than the already deposited snow) (Giddings & LaChapelle, 1961), or that of additional particle deposition, is progressively reduced as the additional layers (of clean snow or new particles) accumulate on the snow surface. Nevertheless, these increase and decrease values are helpful to confirm the close correlation between these features (intensity of traffic and snowfalls) and the snow albedo, and to foresee that any traffic restrictions would be effective to stabilize the conditions of the snowpack in the Chilean Andes near Portillo.

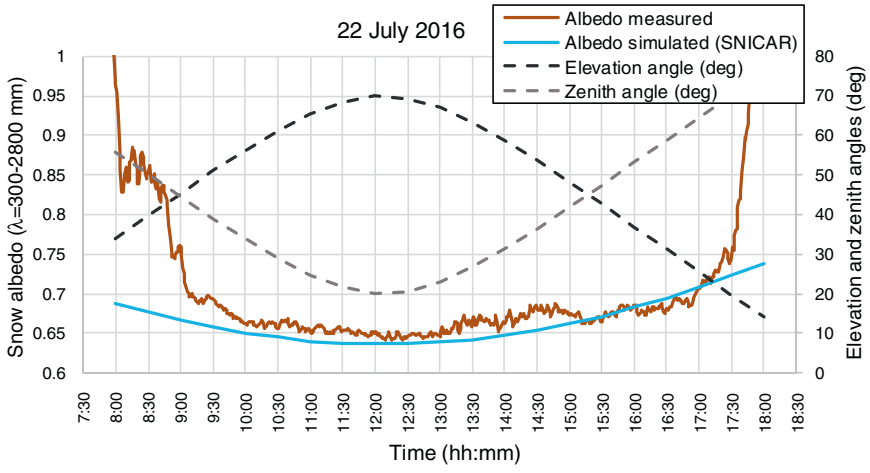

Fig. 10. Modelled and measured broadband daytime snow albedo (solid lines) and elevation and zenith angles (dashed lines) for 22 July.

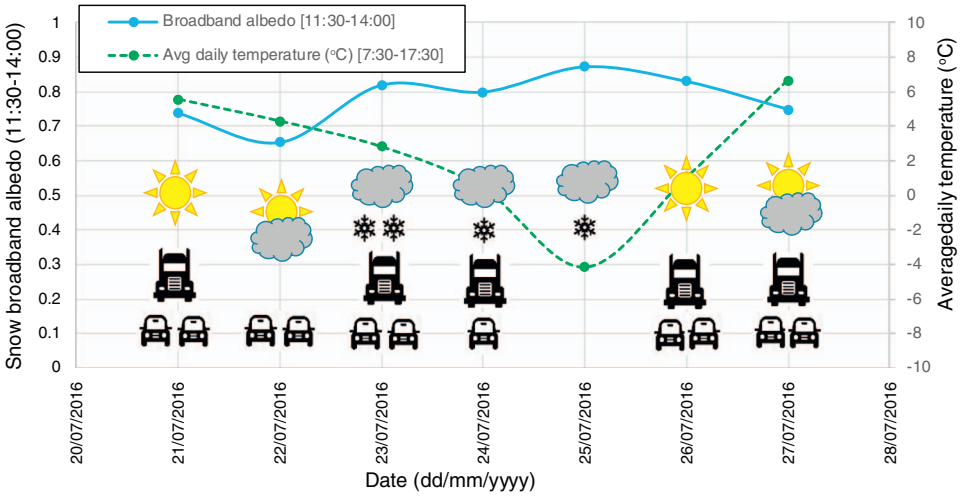

Fig. 11. Midday broadband snow albedo during the measurement campaign.

4. Conclusions

The effect of contamination from vehicles in the surroundings of the Portillo ski resort in the Chilean Andes was assessed from measurements with a radiometer and a weather station located in the Nunatak scientific platform, belonging to CETAM. Results were compared with the snowfall history and the detailed traffic information provided by the Chilean National Service of Customs. A week near the end of July 2016 was selected for the variety of relevant events that occurred, including partial and total traffic restrictions, heavy-short and mild-long snowfalls, sunny and cloudy days and mild and cold temperatures. Wind speed was variable although wind direction was uniform and parallel to the average traffic direction due to terrain restriction, meaning that particle emissions from vehicles were not preferentially blown towards the measuring point. It was observed that the increase in snow albedo after a heavy snowfall (20 cm accumulation) was around 0.17 units, whereas it was only 0.07 after a prolonged lighter snowfall (10 cm accumulation). The mean decrease in albedo observed due to heavy traffic (around 2000 vehicles per day, travelling up and downhill and consuming regular fuels sold in Chile and Argentina) was around 0.08 per day. Although none of these effects is expected to be linear, the observed results suggest that the increase in albedo derived from a light snowfall event (~10 cm) would be approximately compensated within one day by the decrease in albedo derived from intense traffic conditions, and the increase in albedo derived from a heavy snowfall event (~20 cm) would be approximately compensated within two days by the intense traffic-induced albedo decrease. Snow metamorphism and liquid water associated with both ambient temperature and daytime snow-melt may also have contributed to the observed decrease in snow albedo. The daily trends for the snow albedo were confirmed by comparison with the snow albedo modelled with the SNICAR code, for which the albedo of the underlying surface, the snowpack density and thickness, and the grain size, were measured and introduced as inputs. Small differences were attributed to cloudy periods. The albedo changes and their close correlation with traffic intensity and snowfalls are helpful to evaluate the environmental consequences of road traffic on climate change and hydrological cycles in different scenarios. Additional work including measurement of atmospheric black carbon, surface deposition rates, and snow specific surface area and metamorphism is needed for further improvement of our understanding of snow albedo reductions.

Acknowledgements

This research is framed within the Nunatak project, and constitutes the first of a series of studies devoted to evaluate the impact of atmospheric pollutants from anthropogenic activities on snow areas and glaciers, as well as on radiative forcing and climate change. The Nunatak project is funded by Fondo de Protección Ambiental of the Ministry of Environment of Chile and by Center for Environmental Technologies (CETAM), Universidad Técnica Federico Santa María, Valparaíso, Chile. This project was also sponsored by Escuela de Alta Montaña of the Chilean Army and Cresco Energías Renovables Corporation. CONICYT (Chile) is also acknowledged for supporting the visitor stages of Magín Lapuerta, through Programa Atracción de Capital Humano Avanzado Extranjero MEC-Project No 80140096, and of Hans Moosmüller, through project FONDECYT No 1161793. Hans Moosmüller also acknowledges support from NASA EPSCoR under Cooperative Agreement No. NNX14AN24A and from the Desert Research Institute Sabbatical Leave Program.

References

Allen, J.O., Mayo, P.R., Hughes, L.S., Salmon, L.G., Cass, G.R., 2001. Emissions of size-segregated aerosols from on-road vehicles in the Caldecott Tunnel. Environ. Sci. Technol. 35 (21), 4189–4197.
Aoki, T., Hachikubo, A., Hori, M., 2003. Effects of snow physical parameters on shortwave broadband albedos. J. Geophys. Res. 108.
Aoki, T., Kuchiki, K., Niwano, M., Kodama, Y., Hosaka, M., Tanaka, T., 2011. Physically based snow albedo model for calculating broadband albedos and the solar heating profile in snowpack for general circulation models. J. Geophys. Res. 116, D11114.
Brandt, R.E., Warren, S.G., Clarke, A.D., 2011. A controlled snowmaking experiment testing the relation between black carbon content and reduction of snow albedo. J. Geophys. Res. 116, D08109.
Domine, F., Salvatori, R., Legagneux, L., Salzano, R., Fily, M., Casacchia, R., 2006. Correlation between the specific surface area and the short wave infrared (SWIR) reflectance of snow. Cold Reg. Sci. Technol. 46, 60–68.
Dumont, M., Arnaud, L., Picard, G., Libois, Q., Lejeune, Y., Nabat, P., Voisin, P., Morin, S., 2017. In situ continuous visible and near-infrared spectroscopy of an alpine snowpack. Cryosphere 11, 1091–1110.
Flanner, M.G., Zender, C.S., 2006. Linking snowpack microphysics and albedo evolution. J. Geophys. Res.-Atmos. 111 (D12).
Flanner, M.G., Zender, C.S., Hess, P.G., Mahowald, N.M., Painter, T.H., Ramanathan, V., Rasch, P.J., 2009. Springtime warming and reduced snow cover from carbonaceous particles. Atmos. Chem. Phys. 9 (7), 2481–2497.
Gardner, A.S., Sharp, M.J., 2010. A review of snow and ice albedo and the development of a new physically based broadband albedo parameterization. J. Geophys. Res. 115, 1–15.
Giddings, G.C., LaChapelle, E., 1961. Diffusion theory applied to radiant energy distribution and albedo of snow. J. Geophys. Res. 66 (1), 181–189.
Ginot, P., Dumont, M., Lim, S., Patris, N., Taupin, J.D., Wagnon, P., Gilbert, A., Arnaud, Y., Marinoni, A., Bonasoni, P., Laj, P., 2015. A 10 year record of black carbon and dust from a Mera Peak ice core (Nepal): variability and potential impact on melting of Himalayan glaciers. Cryosphere 9, 1685–1699.
Hadley, O.L., Kirchstetter, T.W., 2012. Black-carbon reduction of snow albedo. Nat. Clim. Chang. 2, 437–440.
Hall, A., 2004. The role of surface albedo feedback in climate. J. Clim. 17, 1550–1568.
Hall, A., Qu, X., 2006. Using the current seasonal cycle to constrain snow albedo feedback in future climate change. Geophys. Res. Lett. 33 (L03502), 1–4.
http://snow.engin.umich.edu/snicarcode/. Last accessed 22 September 2017.
http://www.esrl.noaa.gov/gmd/grad/solcalc/azel.html. Last accessed 22 September

2017.
http://www.onthesnow.com/chile/ski-portillo/historical-snowfall.html. Last accessed 22 September 2016.
Jacobi, H.V., Lim, S., Ménégoz, M., Ginot, P., Laj, P., Bonasoni, P., Stocchi, P., Marinoni, A., Arnaud, Y., 2015. Black carbon in snow in the upper Himalayan Khumbu Valley, Nepal: observations and modelling of the impact on the snow albedo, melting and radiative forcing. Cryosphere 9, 1685–1699.
Kondo, J., Yamazawa, H., 1986. Measurement of snow surface emissivity. Bound.-Layer Meteorol. 34, 415–416.
Lee, W.L., Liou, K.N., 2012. Effect of absorbing aerosols on snow albedo reduction in the Sierra Nevada. Atmos. Environ. 55, 425–430.
Manninen, T., Riihela, A., de Leeuw, G., 2012. Atmospheric effect on the ground-based measurements of broadband surface albedo. Atmos. Meas. Tech. 5, 2675–2688.
Ming, J., Cachier, H., Xiao, C., Qin, D., Kang, S., Hou, S., Xu, J., 2008. Black carbon record based on a shallow Himalayan ice core and its climatic implications. Atmos. Chem. Phys. 8, 1343–1352.
Ming, J., Xiao, C., Cachier, H., Qin, D., Qin, X., Li, Z., Pu, J., 2009. Black carbon in the snow of glaciers in China and its potential effects on albedos. Atmos. Res. 92, 114–123.
Moosmüller, H., Chakrabarty, R.K., Arnott, W.P., 2009. Aerosol light absorption and its measurement: a review. J. Quant. Spectrosc. Radiat. Transf. 110 (11), 844–878.
Nolin, A.W., Dozier, J., 2000. A hyperspectral method for remotely sensing the grain size of snow. Remote Sens. Environ. 74, 207–216.
Painter, T.H., Deems, J.S., Belnap, J., Hamlet, A.F., Landry, C.C., Udall, B., 2010. Response of Colorado river runoff to dust radiative forcing in snow. Proc. Natl. Acad. Sci. U. S. A. 107 (40), 17125–17130.
Painter, T.H., Bryant, A.C., Skiles, S.M., 2012. Radiative forcing by light absorbing impurities in snow from MODIS surface reflectance data. Geophys. Res. Lett. 39.
Picard, G., Libois, Q., Arnaud, L., Verin, G., Dumont, M., 2016. Development and calibration of an automatic spectral albedometer to estimate near-surface snow SSA time series. Cryosphere 10 (3), 1297–1316.
Qian, Y., Yasunari, T.J., Doherty, S.J., Flanner, M.G., Lau, W.K.M., Ming, J., Wang, H., Wang, M., Warren, S.G., Zhang, R., 2014. Light-absorbing particles in snow and ice: measurement and modeling of climatic and hydrological impact. Adv. Atmos. Sci. 32, 64–91.
Qu, X., Hall, A., 2007. What controls the strength of snow-albedo feedback? J. Clim. 20, 3971–3981.
Qu, X., Hall, A., 2014. On the persistent spread in snow-albedo feedback. Clim. Dyn. 42, 69–81.
Sterle, K.M., McConnell, J.R., Dozier, J., Edwards, R., Flanner, M.G., 2013. Retention and radiative forcing of black carbon in Eastern Sierra Nevada Snow. Cryosphere 7, 365–374.
Wang, X.W., Zender, C.S., 2010. MODIS snow albedo bias at high solar zenith angles relative to theory and to in situ observations in Greenland. Remote Sens. Environ. 114, 563–575.
www.infoleg.ar. Last accessed 22 September 2017.
www.leychile.cl. Last accessed 22 September 2017.